

LA-UR-02-1502

Approved for public release;
distribution is unlimited.

Title:

Measuring the Stress-Bridging Law of a Heterogeneous Material

Author(s):

C. LIU

Submitted to:

<http://lib-www.lanl.gov/cgi-bin/getfile?00796751.pdf>

Los Alamos National Laboratory, an affirmative action/equal opportunity employer, is operated by the University of California for the U.S. Department of Energy under contract W-7405-ENG-36. By acceptance of this article, the publisher recognizes that the U.S. Government retains a nonexclusive, royalty-free license to publish or reproduce the published form of this contribution, or to allow others to do so, for U.S. Government purposes. Los Alamos National Laboratory requests that the publisher identify this article as work performed under the auspices of the U.S. Department of Energy. Los Alamos National Laboratory strongly supports academic freedom and a researcher's right to publish; as an institution, however, the Laboratory does not endorse the viewpoint of a publication or guarantee its technical correctness.

Measuring the Stress-Bridging Law of a Heterogeneous Material

C. LIU

Materials Science & Technology Division, Los Alamos National Laboratory
Los Alamos, New Mexico 87545, USA

Abstract

In this investigation, fracture experiments on a high explosive material (PBX 9501) were conducted using the digital image correlation technique. From the experimental measurement, we are able to determine quantitatively the stress-bridging law (or decohesion law), which characterizes the relationship between the bridging stress and the opening displacement cross the bridging zone.

1 Introduction

The plastic bonded HMX (PBX) high explosives are composed of the energetic crystal (HMX) and a polymeric binder. Previous experimental observations [1] showed that the fracture process in the sugar mock, a simulant of the PBX 9501 high explosive, is very different from that in brittle solids, even though the high explosive material PBX 9501 is quite brittle under tension. A close examination of the fracture surface revealed that before crack initiation and propagation, a very large damage region is developed ahead of the crack tip. Since such a damage region is very narrow, it can be modeled as a stress bridging zone. Due to the presence of the sizable bridging zone, conventional fracture mechanics is no longer applicable. Stress bridging has to be considered explicitly in order to understand of fracture processes in the PBX 9501 high explosive and the sugar mock.

The model, which explicitly incorporates stress-bridging mechanism, is shown in Fig.1. In describing the model, one would

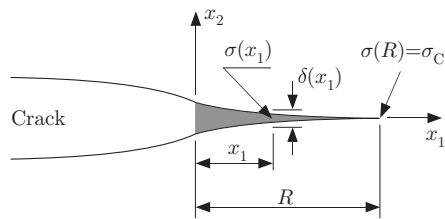


Figure 1: A bridging zone ahead of the crack tip subjected to symmetric loading.

need the following quantities, bridging zone length R , bridging stress $\sigma(x_1)$, bridging-zone opening displacement $\delta(x_1)$, and the critical stress, σ_C , at which bridging zone starts to develop. Among these quantities, the key element for the bridging model is the relationship between the bridging stress σ and the opening displacement cross the bridging zone δ , i.e.,

$\sigma(\delta)$, or the stress-bridging law that can only be determined through experimental measurement.

In this study, fracture experiments on PBX 9501 high explosive using the digital image correlation technique were conducted. From the experimental measurement, we determined quantitatively the stress-bridging law that characterizes the relationship between the bridging stress and the opening displacement cross the bridging zone.

2 Experimental Method

In this section, the digital image correlation technique is briefly summarized, and the PBX 9501 high explosive material and the sample preparation are described.

2.1 Digital image correlation

In this experimental investigation, the digital image correlation technique, as described in [2], is used. Consider an object illuminated by a light source. Suppose that the deformation is planar. Let \mathbb{R} be a small region of the undeformed two-dimensional object and \mathbb{R}_* be the same region but in the deformed configuration. The light intensity pattern of the undeformed region is denoted by $I(\mathbf{x})$ where $\mathbf{x} \in \mathbb{R}$, while the light intensity pattern of the deformed region \mathbb{R}_* is denoted as $I_*(\mathbf{y})$ where $\mathbf{y} \in \mathbb{R}_*$ and $\mathbf{y} = \mathbf{y}(\mathbf{x})$. Both $I(\mathbf{x})$ and $I_*(\mathbf{y})$ are assumed to be in unique and one-on-one correspondence with the respective object surface. If during the deformation process of the small region, the intensity pattern only deforms but does not alter its local value, then we should have

$$I_*(\mathbf{y}) = I_*(\mathbf{y}(\mathbf{x})) = I(\mathbf{x}), \quad \forall \mathbf{x} \in \mathbb{R}. \quad (1)$$

As a result, the measurement of the displacement field using the digital image correlation technique can be formulated into the following mathematical problem: By knowing the two intensity patterns $I(\mathbf{x})$ and $I_*(\mathbf{y})$ of the same region before and after deformation, find a mapping relation $\mathbf{y} = \mathbf{y}(\mathbf{x})$ such that

$$I_*(\mathbf{y}(\mathbf{x})) - I(\mathbf{x}) = \mathbf{0}, \quad \forall \mathbf{x} \in \mathbb{R}. \quad (2)$$

Furthermore, if the deformation is homogeneous, i.e., if the deformation is such that

$$\mathbf{y}(\mathbf{x}) = \mathbf{F}\mathbf{x} + \mathbf{b}, \quad \forall \mathbf{x} \in \mathbb{R}, \quad (3)$$

where \mathbf{F} is a constant tensor and \mathbf{b} is a constant vector. For two-dimensional deformation, the components of \mathbf{F} and \mathbf{b} in

an orthonormal coordinate system can be written as

$$[\mathbf{F}] = \begin{bmatrix} f_{11} & f_{12} \\ f_{21} & f_{22} \end{bmatrix}, \quad [\mathbf{b}] = \begin{bmatrix} b_1 \\ b_2 \end{bmatrix}. \quad (4)$$

The above mathematical problem becomes to find a tensor \mathbf{F} with four scalar components, and a vector \mathbf{b} with two components, such that

$$I_*(\mathbf{F}\mathbf{x} + \mathbf{b}) - I(\mathbf{x}) = \mathbf{0}, \quad \forall \mathbf{x} \in \mathbb{R}. \quad (5)$$

with the restriction of $\det\{\mathbf{F}\} = f_{11}f_{22} - f_{12}f_{21} > 0$. Once the deformation gradient tensor \mathbf{F} and the vector \mathbf{b} are determined, the displacement field in the small region \mathbb{R} is given by

$$\mathbf{u}(\mathbf{x}) = (\mathbf{F} - \mathbf{I})\mathbf{x} + \mathbf{b}, \quad \forall \mathbf{x} \in \mathbb{R}, \quad (6)$$

and the Green-Lagrangian strain tensor within the region \mathbb{R} is

$$\mathbf{E} = \frac{1}{2}(\mathbf{F}^T\mathbf{F} - \mathbf{I}), \quad (7)$$

where \mathbf{I} is the identity tensor.

2.2 Material description and sample preparation

The PBX 9501 high explosive, studied in this investigation, can be viewed as a two-phase composite. It has 95wt% of the cyclotetramethylene-tetranitramine (HMX) crystals and 5wt% of the Estane/nitroplasticizer binder. The microstructure of the PBX 9501 high explosive is shown in Fig.2. To achieve

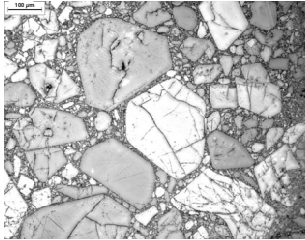


Figure 2: Micrograph of the PBX 9501 high explosive.

such a high volume fraction, the HMX crystal has a very wide spectrum of distribution in size. The diameter of the largest HMX crystal is in the order of $200\mu\text{m}$.

The sample geometry used in this investigation is a modified double-cantilever-beam (DCB) specimen, shown in Fig.3. The length, width, and thickness are 152.4mm, 69.85mm, and 6.35mm, respectively. A notch with 0.508mm in width and 50.8mm in length was cut along the center of the specimen. Meanwhile, in order for the crack to propagate along the center of the specimen, a shallow groove was machined on the back of the specimen and along the center through the entire specimen. The radius of the groove is about 1.58mm. Two loading pins are inserted through the two holes located at one end of the specimen and symmetric with respect to the notch.

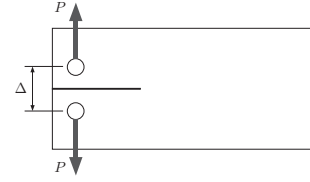


Figure 3: Modified double-cantilever-beam specimen.

A wedge pushes the two loading pins apart and therefore, the notch is opened. A special loading fixture was made to ensure that only the component perpendicular to the notch be transferred to the specimen. An INSTRON load frame was used to load the specimen in displacement control, and the loading speed was set at 0.2mm/min. Before test, a dot-matrix pattern was painted on the surface of the specimen to provide a gray-scale variation, which will be used in the correlation calculations.

3 Experimental Observation and Results

The variation of the applied load, normalized by the thickness of the specimen, versus the separation of the two loading pins is shown in Fig.4. The blue dots represent the moments

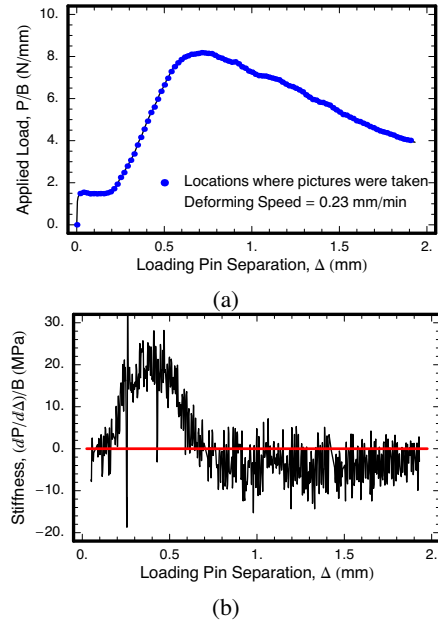


Figure 4: Variations of (a) applied load and (b) specimen stiffness versus opening displacement.

at which the picture of specimen was taken. The initial sudden rise of the load is due to the friction between the wedge and the guiding surface of the loading fixture. This friction does not affect the measurement of the fracture resistance of the sample, since that measurement is based on local calculations. The variation of load as a function of displacement shown in the above figure is typical for the PBX 9501. The

applied load first rises first when the displacement increases. It then reaches a peak value after which the applied load decreases as the displacement continues to increase. In the same figure, we also present the plot of the quantity $(dP/d\delta)/B$ as a function of the separation of the two loading pins. This variation represents the changes of the overall specimen stiffness during the deformation process. The stiffness increases initially, then decreases, and finally becomes negative. At the moment when stiffness drops to zero, the applied load reaches the maximum value. One should notice that the variation of the stiffness is quite smooth (apart from the numerical noise), which is in contrast to most of brittle solids.

The digital image correlation calculations were carried out on the images recorded during the test. In Fig.5, the displacement field and the field of one of the strain components, ϵ_{22} , are presented for the moment at which the applied load has reached its peak value, see Fig.4(a). In Fig.5(c), we see a

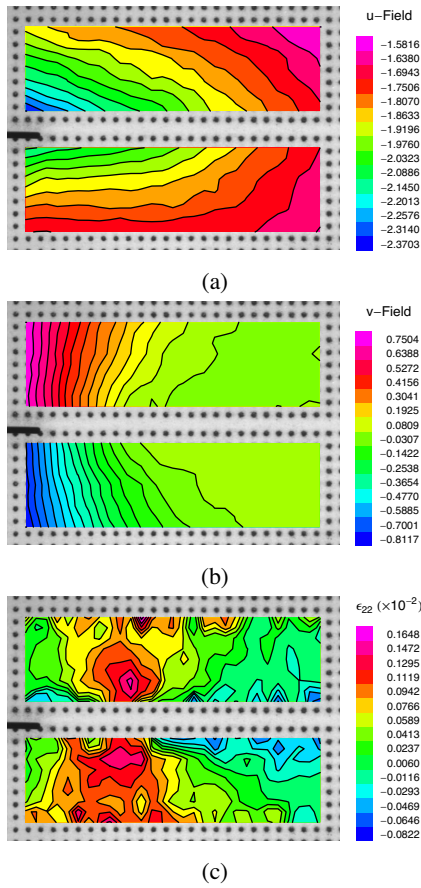


Figure 5: Displacement and strain fields at the moment of peak load.

very high ϵ_{22} region in front of the pre-notch tip, indicating that a bridging zone (or more accurate, a damage zone) has developed. However, there is no visible crack (or material separation) from the images. As the deformation continues to increase, where the applied load follows the descending part of the loading curve, visible crack starts to show. Neverthe-

less, we observe that the high strain region is still ahead of the visible crack tip. Another observation from the captured images is that the crack propagation in PBX 9501 cannot be described as a single point (crack tip) moving continuously through the material. The crack seems jumping ahead in a random fashion and along a zigzag path.

Based on the strain field obtained through the image correlation calculation, and by assuming that the material remains elastic away from the fractured plane, stress field can be calculated at each moment. As a result, the bridging stress can be obtained from the stress component normal to the notch and along the line just above and below the fracture plane. At the same time, the opening displacement cross the fracture plane can be obtained from the displacement result. In Fig.6, the variations of both the opening displacement cross the fracture plane, and the bridging stress as functions of the horizontal coordinate are presented for three arbitrarily chosen moments along the loading curve. The opening displacement

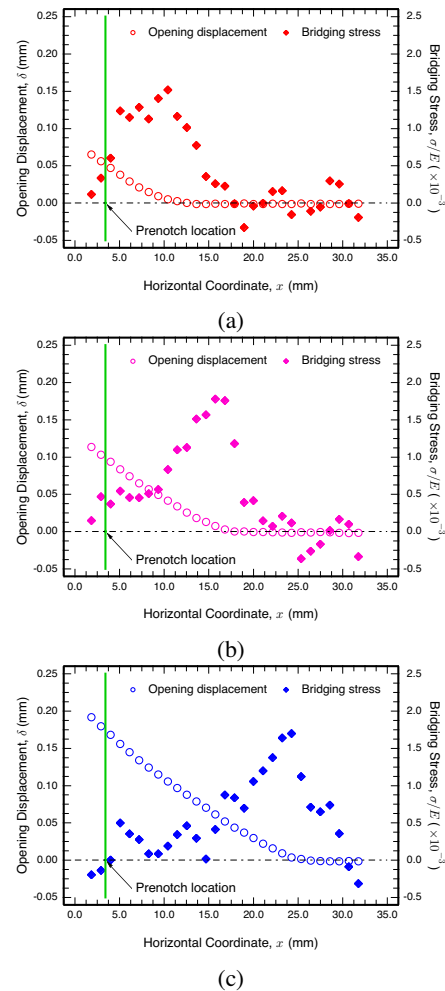


Figure 6: Variations of bridging stress and opening displacement cross the fracture plane.

cross the fracture plane is a monotonic function. Meanwhile, the variations of opening displacement and the bridging stress

show certain degree of correlation indicating that a relationship does exist between the two quantities.

Finally, the variation of the bridging stress as a function of the opening displacement cross the fracture plane is shown in Fig.7 for the three arbitrarily chosen moments. This plot

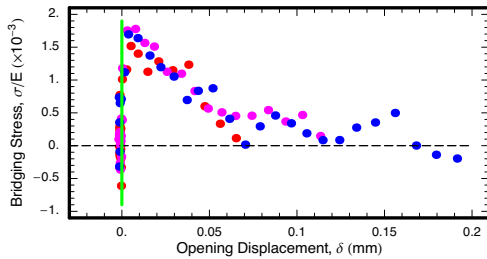


Figure 7: Stress-bridging law of PBX 9501.

represents the stress-bridging law (or decohesion law) for the PBX 9501 high explosive. One observes that the bridging law has a very steep rise portion and reaches the peak at a small opening displacement. This is consistent with the uniaxial tension behavior of the PBX 9501. In tension, PBX 9501 fails at about 0.1% to 0.15% of tensile strain, which is very small compare to compression. After the peak stress, the bridging law has a very long tail, which explains why the classical fracture mechanics approach ceases working for the PBX 9501 and its simulants. Also, the plot indicates that during the test, when the applied load reaches the maximum value, the bridging zone has already fully developed (red dots in the bridging law plot), since the bridging stress has gradually drops to zero at the notch tip.

Based on the stress-bridging law obtained from the fracture experiments, we can study the process of bridging zone initiation, bridging zone enlargement, and crack extension in PBX 9501. Since the rising portion of the stress-bridging law is very steep, we may choose the location where the bridging stress reaches maximum as the location of the bridging zone tip. Also, from the stress-bridging law, we can determine that when the opening displacement cross the bridging zone reaches 0.1mm, the bridging stress drops to zero indication new material surface is generated. In Fig.8(a), the locations of both the bridging zone tip and the crack tip, as function of the separation of the two loading pins are presented. This plot reaffirms the conclusion that the fracture of the PBX 9501 is characterized by the formation and extension of a sizable bridging zone, followed by the crack propagation. From this plot, we see that for the DCB type of configuration, once the crack starts to grow, the stress-bridging zone remains steady state, and the steady-state bridging zone length is in the order of 12mm. If we translate the above plot to the applied load versus displacement curve, shown in Fig.8(b), we can see that the fracture of PBX 9501 follows the sequence of elastic loading, bridging zone enlargement, and crack extension. Moreover, the initiation of the stress-bridging zone occurs before the applied load reaches its maximum value, which suggests

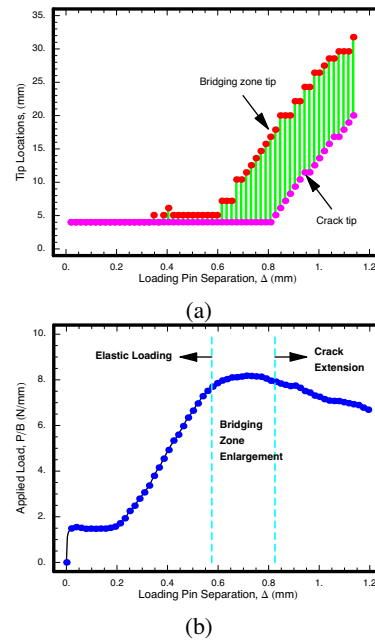


Figure 8: Fracture processes in PBX 9501.

that damage formation and evolution is a dominating factor during the entire deformation process in PBX 9501.

4 Summary

In this investigation, we determined quantitatively the stress-bridging law for the PBX 9501 high explosive under quasi-static loading conditions. The stress-bridging law governs how fracture would occur in the material and it is a material property similar to the elastic constants and other material parameters. It is believed that the stress-bridging law will also depends on the loading rate, temperature, and other ambient conditions. The effect of these conditions on the fracture behavior of PBX 9501, is currently pursued.

Acknowledgements

This research was supported financially by the US Department of Energy and the Department of Defense/Office of Munitions under the Joint DoD/DOE Munitions Technology Development Program. The author would also like to thank Messrs. R.W. Ellis, E.L. Roemer, and W.J. Wright of Los Alamos National Laboratory, for the assistance in conducting the experiments presented in this study.

References

- [1] Liu, C., Stout, M.G. and Asay, B.W., "Stress bridging in a heterogeneous material," *Engineering Fracture Mechanics*, **67**, pp.1–20, (2000).
- [2] Chu, T.C., Ranson, W.F., Sutton, M.A. and Peters, W.H., "Applications of digital image correlation techniques to experimental mechanics," *Experimental Mechanics*, **25**, pp.232–244, (1985).